ARTICLE
Traditional Medicine Research 2027;12(1):2. https://doi.org/10.53388/TMR2027002

Integration of network pharmacology and metabolomics to elucidate Qi-Xiong-Qu-Yu decoction mitigates myocardial ischemia via regulating Nrf2/ROS/MAPK signaling

Li-Ping Chen[1#], Hang-Hang Gou[1#], Cheng-Xun He[1, 2], Ya-Mei Wu[3], Wei Peng[1*], Yun-Hui Chen[1*], Jun Chen[2*]

[1]School of Pharmacy, School of Basic Medical Sciences, CDUTCM-KEELE Joint Health and Medical Sciences Institute, Chengdu University of Traditional Chinese Medicine, Chengdu 611137, China. [2]Hospital of Chengdu University of Traditional Chinese Medicine, Chengdu University of Traditional Chinese Medicine, Chengdu 610032, China. [3]Sichuan Academy of Chinese Medicine Sciences, Chengdu 610041, China.

[#]These authors contributed equally to this work and are co-first authors for this paper.
[*]**Correspondence to:** Wei Peng, Yun-Hui Chen, School of Pharmacy, School of Basic Medical Sciences, CDUTCM-KEELE Joint Health and Medical Sciences Institute, Chengdu University of Traditional Chinese Medicine, No. 1166, Liutai Avenue, Chengdu 611137, China. E-mail: pengwei@cdutcm.edu.cn; cyhcdutcm@163.com. Jun Chen, Hospital of Chengdu University of Traditional Chinese Medicine, Chengdu University of Traditional Chinese Medicine, No. 39, Shierqiao Road, Chengdu 610032, China. E-mail: drchenjun@qq.com.

Abstract

Background: Qi-Xiong-Qu-Yu decoction (QXD) is an empirical herbal formula developed for the clinical treatment of ischemic heart disease. **Methods:** Isoproterenol (ISO) was used to establish a rat model of myocardial ischemia, and the effects of QXD were evaluated. The chemical profile of QXD was identified using UPLC-Q-Exactive-MS. Network pharmacology was then performed based on the UPLC-MS identified constituents and GEO datasets, and plasma metabolomics was employed to predict the molecular signaling. Finally, cell and animal experiments were conducted to verify the predicted results. **Results:** QXD exerted therapeutic effects in ISO-induced myocardial ischemia rats. A total of 23 constituents were identified in QXD via UPLC-MS. Integrated network pharmacology and metabolomics analyses indicated that regulation of the Nrf2/ROS/MAPK pathway may underlie the anti-myocardial ischemia effects of QXD. In vivo, QXD significantly lowered the elevated serum levels of myocardial injury biomarkers (cTnT, CK-MB, and LDH) and decreased myocardial MDA levels, attenuated cardiomyocyte apoptosis and myocardial fibrosis, and restored the activities of antioxidant enzymes including SOD and GSH-Px. In vitro, QXD reduced the release of cTnT, CK-MB, and LDH into the cell culture supernatant, decreased intracellular ROS and MDA levels, and increased SOD activity in ISO-stimulated H9C2 cells. Our study suggests that the cardioprotective effects of QXD may be mediated by promoting the nuclear accumulation of Nrf2, which upregulates the expression of antioxidant enzymes, thereby inhibiting the activation of MAPK signaling. **Conclusion:** QXD mitigated ISO-induced myocardial ischemia in rats, and the underlying molecular mechanisms are closely associated with the suppression of cardiomyocyte apoptosis via the Nrf2/ROS/MAPK pathway.

Keywords: Qi-Xiong-Qu-Yu decoction; myocardial ischemia; network pharmacology; metabolomics; Nrf2/ROS/MAPK signaling; cell apoptosis

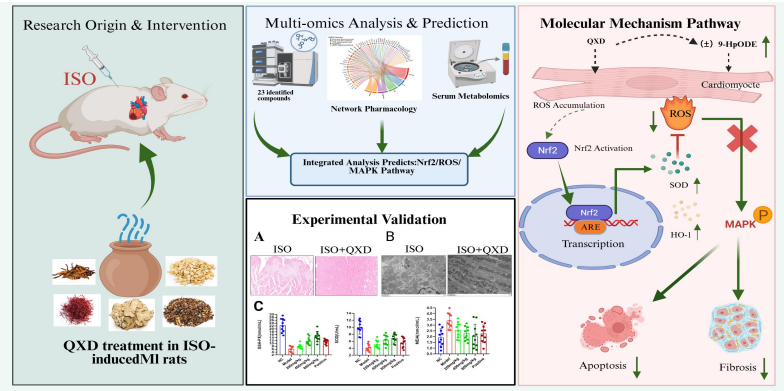

Author contributions

Peng W, Chen YH, and Chen J contributed to the conceptualization, reviewing, and editing of the manuscript. Chen LP, Gou HH, and He CX performed the experiments, curated the data, and prepared the original draft. Wu YM and Chen J contributed to the methodology and supervised the study.

Competing interests

The authors declare no conflicts of interest.

Acknowledgments

This work was supported by Sichuan Science and Technology Program (No. 2025ZNSFSC0582), International Cooperation and Exchange Project of Science & Technology Department of Sichuan Province (No. 23GJHZ0100, 2017HH0004), and Sichuan Provincial Administration of Traditional Chinese Medicine (No. 2021MS464).

Peer review information

Traditional Medicine Research thanks Chuan Wang, Han-Qing Pang and other anonymous reviewers for their contribution to the peer review of this paper.

Abbreviations

9-HpODE, 9(S)-hydroperoxy-10(E),12(Z)-octadecadienoic acid; Bax, Bcl-2-associated X protein; Bcl-2, B-cell lymphoma-2; CK-MB, creatine kinase-MB isoenzyme; cTnT, cardiac troponin T; DAPI, 4′,6-diamidino-2-phenylindole; DEGs, differentially expressed genes; FC, fold change; GO, Gene Ontology; GSH-Px, glutathione peroxidase; H&E, hematoxylin and eosin; ISO, isoproterenol; JNK, c-Jun N-terminal kinase; KEGG, Kyoto Encyclopedia of Genes and Genomes; LDH, lactate dehydrogenase; MAPK, mitogen-activated protein kinase; MDA, malondialdehyde; Nrf2, nuclear factor erythroid 2-related factor 2; PARP1, poly(ADP-ribose) polymerase 1; PCA, principal component analysis; PI, propidium iodide; QXD, Qi-Xiong-Qu-Yu decoction; ROS, reactive oxygen species; RT, retention time; SD, standard deviation; SOD, superoxide dismutase; TCM, traditional Chinese medicine.

Citation

Chen LP, Gou HH, He CX. Integration of network pharmacology and metabolomics to elucidate Qi-Xiong-Qu-Yu decoction mitigates myocardial ischemia via regulating Nrf2/ROS/MAPK signaling. *Tradit Med Res.* 2027;12(1):2. doi: 10.53388/TMR2027002.

Editorial advisory board: Yi Ding.
Production editor: Na Liu and Xiao-Han Li.
Received: 30 June 2026; **Revised:** 14 August 2026; **Accepted:** 28 August 2026; **Available online:** 31 August 2026.
© 2027 By Author(s). Published by TMR Publishing Group Limited.
This is an open access article under the CC-BY license.
(https://creativecommons.org/licenses/by/4.0/)

Highlights

1. Qi-Xiong-Qu-Yu decoction (QXD) mitigates isoproterenol-induced myocardial ischemia by suppressing cardiomyocyte apoptosis and myocardial fibrosis.
2. The Nrf2/ROS/MAPK signaling axis serves as the potential mechanism underlying the cardioprotective effects of QXD.
3. Upregulation of the endogenous metabolite 9-HpODE may also be an important mechanism underlying the cardioprotective effects of QXD

Medical history of objective

Qi-Xiong-Qu-Yu decoction (QXD) is a clinically proven formula developed based on the classical principle of "invigorating Qi and promoting blood circulation," a principle exemplified by Buyang Huanwu Decoction, which was first documented in *Yi Lin Gai Cuo* (1830 C.E.) by Qingren Wang of the Qing Dynasty. Its primary efficacies lie in invigorating Qi, promoting blood circulation, removing blood stasis, and dredging collaterals; accordingly, it is clinically applied to treat "thoracic obstruction," which corresponds to myocardial ischemia in modern medicine. Modern research has revealed that QXD and its component herbs exhibit multiple pharmacological effects, including antioxidative, anti-inflammatory, and anti-apoptotic properties, as well as cardioprotective activities.

Introduction

Coronary artery disease (CAD), the predominant etiology of ischemic heart disease (IHD), represents a critical global health burden, contributing to over nine million deaths annually due to compromised cardiac blood supply [1, 2]. With an aging population, the incidence and associated socioeconomic impact of myocardial ischemia continue to rise, underscoring an urgent need for more effective therapeutic strategies [3, 4]. Contemporary clinical management primarily relies on pharmacotherapies such as antiplatelet agents and β-blockers. However, their clinical efficacy may vary among different patient populations [5, 6], highlighting a significant unmet clinical need for safer and more holistic therapeutic alternatives.

Traditional Chinese medicine (TCM), guided by the principles of the “holistic concept” and “treatment based on syndrome differentiation” offers a distinct therapeutic paradigm with demonstrated potential in managing complex, multi-factorial diseases, including cardiovascular disorders [7–9]. Correspondingly, Qi-Xiong-Qu-Yu decoction (QXD) is a clinically experienced, self-designed formula with the functions of “*invigorating Qi, promoting blood circulation, removing blood stasis and dredging collaterals*”, comprising seven herbal medicines: the roots of *Astragalus membranaceus* (Fisch.) Bunge, the rhizomes of *Ligusticum chuanxiong* Hort., the roots of *Paeonia lactiflora* Pall., the flowers of *Carthamus tinctorius* L., Cordyceps, the semen of *Prunus persica* (L.) Batsch, and the bark of *Cinnamomum cassia* (L.) D. Don. In the QXD formula , the monarch drug was the roots of *A. membranaceus*, increasing evidence has suggested that roots of *A. membranaceus* contain abundant triterpenes and flavonoids which possess good anti-oxidative, anti-inflammatory, and cardiomyocyte protection activities [10, 11]. Besides, it’s reported that other herbal medicines, such as roots of *L. chuanxiong* and flowers of *C. tinctorius*, also have significant cardiomyocyte protection activities [12, 13]. Nowadays, QXD has been used to treat various cardiovascular diseases in clinical, in particular for the ischemic heart diseases. However, so far, it remains unknown what are the active substances in QXD for therapeutical effects against ischemic heart diseases, let alone the underlying pharmacological mechanisms.

Emerging research evidence suggests that integration of network pharmacology and metabolomics is a versatile *in-silico* way for holistic exploration the active substances and underlying molecular mechanisms of TCMs and their formulas [14, 15]. Consequently, to bridge traditional wisdom with contemporary systems biology, this study carried out an integrative approach of network pharmacology and metabolomics to holistically clarify the scientific connotation regarding therapeutical effects of QXD against ischemic heart diseases, thereby affording a robust scientific foundation for its optimized clinical application and future new drug development.

Methods

Materials and chemicals

All the herbal medicines in QXD were obtained from the Sichuan Neautus traditional Chinese medicine, Co., Ltd. (https://www.xinhehua.com/sy, Chengdu, China) and were identified by Professor Wei Peng (School of Pharmacy, Chengdu University of TCM, Chengdu, China). The sources of main chemical reagents, anti-bodies and testing kits were summarized in Supplementary Tables S1 and S2.

UPLC-Q-Exactive Orbitrap-MS analysis

QXD consists of the following crude drugs: *Astragalus membranaceus* (Fisch.) Bge. (root, 10 g), *Ligusticum chuanxiong* Hort. (rhizome, 6 g), *Paeonia lactiflora* Pall. (root, 5 g), *Carthamus tinctorius* L. (flower, 5 g), *Cordyceps sinensis* (Berk.) Sacc. (fruiting body, 6 g), *Prunus persica* (L.) Batsch (seed, 5 g), and *Cinnamomum cassia* Presl (bark, 5 g). All herbal materials were authenticated according to the Chinese Pharmacopoeia (2025 edition) and voucher specimens were deposited at the Chengdu University of Traditional Chinese Medicine Museum. The herbal medicines were mixed and powdered, and then 10 g QXD powder was extracted by reflux with 100 mL 70% ethanol for 1 h. After filtration, ethanol was removed under reduced pressure, and the extract was subsequently freeze-dried. Then, the freeze-dried powder was re-dissolved in 100 mL MeOH, and filtrated through 0.22 μm membrane to afford the testing sample of the ultra-performance liquid chromatography (UPLC)-Q-Exactive Orbitrap-MS analysis (Thermo Fisher Scientific, Waltham, MA, USA). The used chromatographic column was C18 reversed-phase column (Thermo Hypersil GOLDTM, 100 mm × 2.1 mm, 1.9 μm), and the detail mobile phase information and mass spectrometry conditions were summarized in Supplementary Tables S3 and S4, respectively.

Network pharmacology study

Hub target genes for anti-myocardial ischemia effects of QXD. The chemical constituents of QXD were characterized by UPLC-Q-Exactive-MS analysis. Potential protein targets of the identified compounds were systematically retrieved from multiple publicly accessible online databases (Supplementary Table S5), including PharmMapper, Swiss Target Prediction, TCMSP, and CTD. After intergrating the results from all sources and the removing duplicates, a comprehensive target set for QXD was established.

Three myocardial ischemia-related microarray datasets (GSE48060, GSE66360, and GSE97320) were retrieved from the Gene Expression Omnibus (GEO) database (Supplementary Table S6). The search was limited to “Homo sapiens” and “expression profiling by array”. These datasets comprised a total of 157 samples, including 83 myocardial ischemia samples and 74 control samples. Raw data (CEL files) were background-corrected, normalized, and summarized using the robust multi-array average (RMA) algorithm. Probe IDs were converted to gene symbols based on the GPL570 platform annotation file. To mitigate non-biological variations introduced by merging multiple datasets, the ComBat function from the sva R package was employed for batch effect correction and the effectiveness of the correction was evaluated by principal component analysis (PCA).

Differential expression analysis between myocardial ischemia and control groups on the batch corrected expression matrix using the limma R software package. Among them, genes with an adjusted

P-value (false discovery rate, FDR) < 0.05 and $|\log_2 FC| \geq 0.5$ were considered as significantly differentially expressed genes (DEGs). To avoid missing genes related to diseases but with insignificant expression differences in differential gene analysis, we also conducted WGCNA analysis by reducing the entire set of genes into multiple modules and selecting the module most relevant to phenotype as the key gene. Subsequently, the DEGs and key genes were merged to construct a disease-related gene set for downstream analysis. Finally, the hub target genes mediating the anti-myocardial ischemia effects of QXD were identified by intersecting the disease-related genes with the predicted QXD-related targets.

Enrichment analysis. To investigate the key signaling pathways and biological functions of the core targets, Gene Ontology (GO) and Kyoto Encyclopedia of Genes and Genomes (KEGG) enrichment analyses were performed using clusterProfiler (version 4.8.3) in R (version 4.3.1) / the online Database for Annotation, Visualization and Integrated Discovery (DAVID, https://david.ncifcrf.gov/, version 6.8) / Metascape (https://metascape.org/). The input gene list comprised the core therapeutic targets obtained from the intersection of differentially expressed genes (DEGs) and key WGCNA module genes. Homo sapiens was selected as the reference species, and gene symbols were converted to Entrez IDs using the org.Hs.eg.db annotation package prior to analysis. GO enrichment analysis covered three categories: biological process (BP), cellular component (CC), and molecular function (MF). KEGG pathway enrichment analysis was conducted against the KEGG database. Statistical significance was defined as an adjusted P-value (Benjamini–Hochberg false discovery rate, FDR) < 0.05 and a minimum count of enriched genes ≥ 3. The enrichment results were visualized using the ggplot2 package [16].

Animal investigations

Animals and ISO-induced myocardial ischemia rat model. Sixty male Sprague-Dawley (SD) rats (6 weeks old, weighing 180–220 g) were purchased from SPF (Beijing) Biotechnology Co., Ltd. (license No. SCXK (Jing) 2024-0001) and housed under specific pathogen-free (SPF) conditions at 20–25 °C with 50–60% humidity and a 12 h light/dark cycle, with free access to standard chow and water. The 60 rats were randomly assigned into 6 groups (n = 10): normal control (NC), model, QXD (200, 400, and 800 mg/kg), and positive control (propranolol, 10 mg/kg) groups. The doses of QXD were determined according to the clinically equivalent dose converted by body surface area normalization (conversion coefficient of 6.3 for rats) and our preliminary experiments, with 400 mg/kg corresponding to the clinical equivalent dose of the QXD extract. Propranolol, administered orally (p.o.) at 10 mg/kg, was used as the positive control, and the dose was selected based on previous studies [17, 18]. Rats in the QXD and positive control groups were orally administered QXD or propranolol for 2 weeks. On days 13 and 14, 30 min after drug administration, all rats except those in the normal group were intraperitoneally (i.p.) injected with isoproterenol (ISO, 85 mg/kg) to establish the myocardial ischemia model [19, 20]. ISO was injected for 2 consecutive days, and the normal group received an equal volume of normal saline intraperitoneally (Figure 1A). Twenty-four hours after the last ISO injection, all rats were anesthetized with sodium pentobarbital (45 mg/kg, i.p.) and euthanized by exsanguination (via the abdominal aorta), and the hearts were rapidly excised, rinsed with ice-cold normal saline, and either fixed in 4% paraformaldehyde or snap-frozen in liquid nitrogen and stored at –80 ℃ for subsequent histological, ultrastructural, and molecular analyses. All animal experiments were approved by the Experimental Animal Welfare and Ethics Committee of Chengdu University of Traditional Chinese Medicine (approval no. 2025111) and were conducted in strict accordance with the ARRIVE guidelines.

H&E and Masson staining. Heart tissue specimens were harvested, and fixed in 4% paraformaldehyde buffered solution for 24 h, followed by paraffin embedding according to standard histological protocols. The paraffin blocks were sectioned at a thickness of 5 μm and stained with hematoxylin and eosin (H&E). Adjacent sections were also stained with a Masson's trichrome kit, and cardiac pathological changes were evaluated under a microscope (Nikon TS2, Tokyo, Japan).

TUNEL assay. To detect the cell apoptosis in cardiac tissues, the cardiac sections were processed using a one-step TUNEL apoptosis kit according to the manufacturer's instructions. After dewaxing and rehydration in graded ethanol, the sections were treated with proteinase K (20 μg/mL, 5 min). The TdT enzyme-labeling mixture was then applied, followed by incubation at 37 °C for 60 min under humidified conditions.

TEM analysis. The animals were humanely euthanized and subsequently perfused transcardially with 50 mL of sterile 0.9% NaCl solution, immediately followed by 100 mL of 2.5% glutaraldehyde fixative in cacodylate buffer (pH 7.3, 0.1 M). Apical myocardial specimens were post-fixed, dehydrated through a graded ethanol series (50%–100%) and acetone, and then embedded in epoxy resin (Epon 812). Ultrathin sections (70 nm) were prepared according to previously reported methods [21]. Ultrastructural analysis was performed using an HT7800 transmission electron microscope (TEM) (Hitachi High-Tech, China) operated at an accelerating voltage of 80 kV.

Determination of myocardial injury biomarkers. Blood samples and cell supernatants were centrifuged (3,000× g, 15 min, 25 °C) to obtain serum and supernatants, respectively. The concentrations of serum creatine kinase-MB isoenzyme (CK-MB), lactate dehydrogenase (LDH), and cardiac troponin T (cTnT) were determined using ELISA kits.

Determination of myocardial oxidative stress indexes. Cardiac oxidative stress biomarkers, including malondialdehyde (MDA), glutathione peroxidase (GSH-Px) and superoxide dismutase (SOD), were quantitatively analyzed in myocardial homogenates using standardized colorimetric methods in accordance with the manufacturers' instructions.

Western blotting assay. For total protein extraction, Cardiac tissue or cells lysates were prepared using RIPA buffer (Thermo Fisher Scientific, Shanghai, China). For nuclear and cytoplasmic fractionation, cells were lysed using the NE-PER Nuclear and Cytoplasmic Extraction Reagents (Thermo Fisher Scientific) according to the manufacturer's instructions. Briefly, cells were washed with ice-cold PBS and incubated in CER I buffer for 10 min on ice, followed by the addition of CER II buffer and centrifugation (16,000× g, 5 min, 4 °C) to collect the cytoplasmic extract. The remaining nuclear pellet was resuspended in NER buffer, vortexed (15 sec, every 10 min, 4 times, on ice), and centrifuged (16,000× g, 10 min, 4 °C) to obtain the nuclear extract. Protein aliquots (30 μg/lane) were separated by electrophoresis on 10% SDS-PAGE gels and then transferred onto PVDF membranes. The membranes were blocked with 5% BSA and probed with primary antibodies, followed by incubation with HRP-conjugated secondary antibodies. Finally, the protein bands were visualized by chemiluminescence using an imaging system (Bio-Rad Laboratories, Hercules, CA, USA) with ECL substrate. Densitometric analysis was performed using ImageJ 1.53a. Cytoplasmic Nrf2 was normalized to β-actin, nuclear Nrf2 was normalized to Lamin B1, and p38 as well as phosphorylated p38 (p-p38) were normalized to GAPDH. Other total protein levels were normalized to β-actin.

Metabolomics study

SD rats were randomly divided into two groups (n = 6 per group): the model group and the treatment group. Rats in the treatment group were orally administered QXD at a dose of 800 mg/kg by gavage once daily for 2 consecutive weeks, while rats in the model group received an equal volume of vehicle. Myocardial ischemia was induced as described in the animal experiment section. At the end of the experiment, blood samples were collected from the abdominal aorta under anesthesia, and plasma samples were collected and stored at −80 °C until analysis. A pooled quality control (QC) sample was prepared by mixing equal aliquots of each plasma sample and processed identically to the experimental samples to monitor system stability and data reproducibility. For metabolite extraction, a 100 μL aliquot of plasma was transferred to an EP tube, mixed with 400 μL of

80% (v/v) aqueous methanol, and vortex-mixed thoroughly. After incubation on ice for 5 min, the mixture was centrifuged (15,000 × g, 20 min, 4 °C), and the supernatant was collected. Metabolomics analysis was then conducted by Novogene Co., Ltd. (https://cn.novogene.com/, Beijing, China). Briefly, the supernatant was diluted with water to a final methanol content of 53%, followed by re-centrifugation under identical conditions. The processed supernatant was analyzed via UPLC-Q-Exactive Orbitrap-MS using a Hypersil Gold C18 column with the mobile phase parameters listed in Supplementary Table S7, and the detailed MS conditions are summarized in Supplementary Table S8. QC samples were injected at the beginning of the analytical run, after every 10 experimental samples, and at the end of the batch to ensure instrument stability and data reliability.

The raw datasets were processed using Compound Discoverer 3.1 software for preliminary metabolite characterization based on the retention time (RT), mass-to-charge ratio (m/z), and associated chromatographic parameters. Chromatographic peaks were aligned with tolerances of 0.2 min (RT) and 5 ppm (mass accuracy). Strict peak extraction criteria were applied, including a mass deviation of ≤ 5 ppm, an intensity variance of < 30%, a signal-to-noise ratio of ≥ 3, minimum intensity thresholds, and ion summation-based quantification. Molecular formula prediction integrated MS/MS fragmentation patterns cross-referenced against mzCloud™, mzVault, and Masslist databases. Background interference was eliminated through blank sample subtraction prior to data normalization. Data processing was performed on a Linux CentOS 6.6 platform using R and Python.

Metabolite annotation was performed by cross-referencing with the KEGG, HMDB, and LIPIDMAPS databases. Multivariate analysis was conducted using partial least squares-discriminant analysis (PLS-DA), and variable importance in projection (VIP) scores were obtained. Complementary univariate analysis employed Student's t-tests to determine probability values (P) and fold change (FC) metrics. Differential metabolites were selected using established thresholds: VIP > 1.0, $P < 0.05$ (two-tailed), and FC ≥ 2.0 or ≤ 0.5. To integrate the findings of network pharmacology and metabolomics, joint pathway analysis was performed using the Joint Pathway Analysis module of MetaboAnalyst 5.0 (https://www.metaboanalyst.ca/). The 329 core targets and the 14 differential metabolites (as KEGG compound IDs) were simultaneously input, with Homo sapiens selected as the reference organism, and pathway enrichment was evaluated against the KEGG database.

Cell culture

H9C2 cells were purchased from Wuhan Sunncell Biotechnology Co., Ltd. (Wuhan, China; catalog no. SNL-029) and cultured in DMEM containing 10% FBS (37 °C, 5% CO_2). The ISO-stimulated H9C2 cell model was established by treating cells with 100 μM ISO for 24 h [22], and the working concentration of QXD was determined by dose-response experiments: H9C2 cells were pretreated with QXD (1.25–120 μg/mL) for 24 h, followed by ISO stimulation, and cell viability was assessed by the CCK-8 assay. QXD increased the viability of H9C2 cells in a dose-dependent manner, with the most pronounced protection against ISO-induced injury at 100 μg/mL (Supplementary Figure S3); therefore, 100 μg/mL was selected as the working concentration of QXD.

Apoptosis assays

Cell apoptosis was detected by flow cytometry analysis with Annexin V-FITC/PI staining (4A BIOTECH, Suzhou, China) Cells were cultured in 6-well plates and treated with ISO and QXD, then the cells were harvested and analyzed by flow cytometry analysis (BD Biosciences, Shanghai, China) with Annexin V-FITC/PI staining as previously described [23].

Oxidative stress determination

Oxidative stress was assessed by confocal microscopy with DCFH-DA staining. Briefly, H9C2 cells were cultured on glass-bottom confocal dishes and treated with ISO and QXD; the cells were then stained with 10 μM DCFH-DA in serum-free medium at 37 °C for 30 min in the dark. After washing with PBS three times, the cells were observed under a confocal microscope. In addition, intracellular MDA and SOD levels were determined using commercial kits as described above.

Nrf2 nuclear accumulation assays

Immunofluorescence staining was conducted to examine the subcellular localization of Nrf2 in H9C2 cells. Briefly, cells were seeded in glass-bottom confocal dishes and subjected to the aforementioned modeling and drug treatment protocols. After treatment, cells were fixed with 4% paraformaldehyde for 15 min at room temperature, permeabilized with 0.1% Triton X-100 for 10 min, and blocking with 3% bovine serum albumin (BSA) for 1 h at room temperature. The cells were incubated with a primary antibody against Nrf2 (1:100) overnight at 4 °C. Following three washes with PBS, the cells were incubated with an Alexa Fluor 488-conjugated goat anti-rabbit IgG secondary antibody (1:200) for 1 h at room temperature in the dark. Nuclei were counterstained with DAPI for 10 min at room temperature in the dark, and images were acquired using a confocal microscope. Nrf2 nuclear accumulation was quantified using ImageJ software (NIH) by measuring the mean fluorescence intensity of Nrf2 in the nucleus and cytoplasm, respectively. The nuclear-to-cytoplasmic (N/C) fluorescence intensity ratio was calculated for each cell, and at least 50 randomly selected cells per group were analyzed.

Statistical analysis

Data are presented as mean ± SD. Normality and variance homogeneity were confirmed by the Shapiro-Wilk and Brown-Forsythe tests, respectively. Intergroup differences were then analyzed using one-way ANOVA followed by Tukey's HSD post hoc test. Statistical significance was set at $P < 0.05$. Analyses were conducted with GraphPad Prism 10.0 (GraphPad Software, San Diego, CA, USA).

Results

QXD Mitigated myocardial injury in ISO induced myocardial ischemia rats

As shown in Figure 1B–1D, ISO induction could significantly increase the serum levels of myocardial injury biomarkers including cTnT, CK-MB and LDH in myocardial ischemia rats, compared with the normal rats (NC). Notably, QXD treatment (200, 400, and 800 mg/kg) significantly reversed the elevation of these enzymes in the serum of myocardial ischemia rats ($P < 0.05$). Furthermore, pathological changes in the myocardial tissues of myocardial ischemia rats were examined by H&E staining. As shown in Figure 1E, myocardial cells in normal rats were arranged in an orderly manner with clear structures, and no obvious pathological changes were observed. In contrast, after ISO induction, extensive degeneration and necrosis of myocardial cells were observed, accompanied by inflammatory cell infiltration, fibrous tissue hyperplasia in the necrotic areas, and hemorrhage with red blood cell extravasation. These pathological injuries were alleviated in QXD-treated myocardial ischemia rats. In addition, Masson's trichrome staining was performed to evaluate myocardial fibrosis (Figure 1F). Consistent with the H&E staining results, obvious myocardial fibrosis was observed in the myocardial tissues of myocardial ischemia rats after ISO stimulation, whereas QXD treatment appeared to ameliorate the degree of fibrosis.

Identification of the main constituents in QXD via UPLC-Q-Exactive Orbitrap-MS

The main constituents of QXD were analyzed using UPLC-Q-Exactive Orbitrap-MS. As shown in Figure 2A, 2B and Table 1, a total of 23 compounds were identified in QXD, including safflomin A (10.44 min), amygdalin (10.51 min), trans-Cinnamaldehyde (15.20 min), albiflorin (15.23 min), glycitin (18.67 min), rutin (19.36 min),

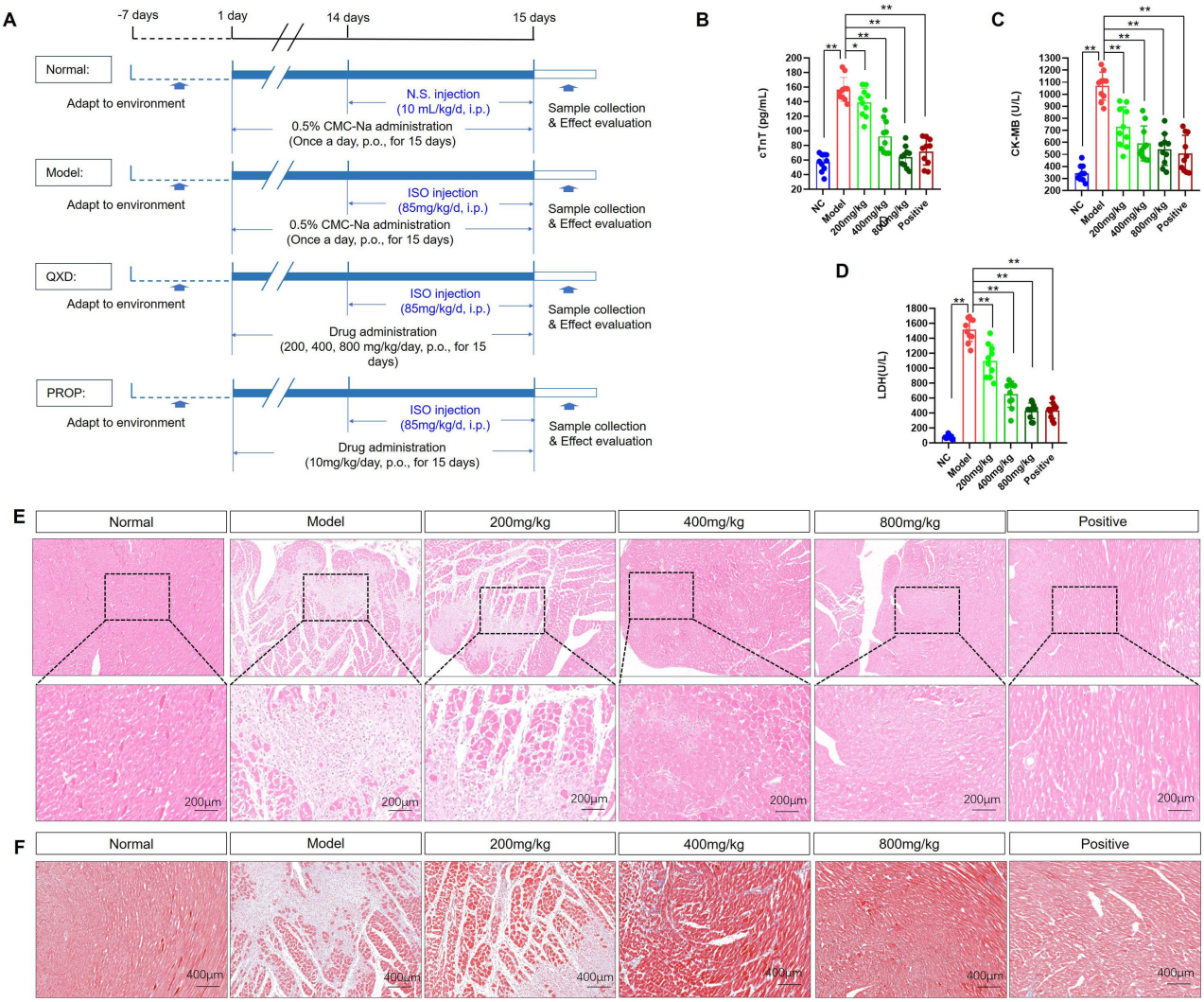

Figure 1 Effects of QXD on myocardial ischemia in rats.
(A) The workflow design of animal experiments. (B–D) myocardial injury biomarkers levels of cTnT, CK-MB, and LDH in serum of the myocardial ischemia rats; (E, F) Pathological examinations of the myocardial tissues in myocardial ischemia rats with HE staining and Masson staining. Data were expressed as mean ± SD (n = 10), $^{*}P < 0.05$, $^{**}P < 0.01$ vs. Model group. NC, normal control; cTnT, cardiac troponin T; CK-MB, creatine kinase-MB; LDH, lactate dehydrogenase; QXD, Qi-Xiong-Qu-Yu decoction; PROP, propranolol; N.S., normal saline; i.p., intraperitoneal; p.o., per os.

3',4',7-Trihydroxyflavanone (22.95 min), senkyunolide H (23.45 min), ononin (24.85 min), eriodictyol (26.35 min), methylnissolin-3-O-glucoside (26.90 min), benzoylpaeoniflorin (29.00 min), astragaloside IV (30.30 min), formononetin (30.97 min), 5,7-Dihydroxy-3-(4-methoxyphenyl)-4H-chromen-4-one (32.90 min), 6-Gingerol (33.00 min), senkyunolide A (33.75 min) and levistilide A (40.95 min), *etc*. Collectively, the main components in QXD included organic acids (32.56%), flavonoids (23.26%), amino acids (11.63%), lignans (10.47%), nucleosides (6.98%), butylphthalides (3.49%), and terpenoids (3.49%), *etc*. (Figure 2C).

Combining differential gene analysis and WGCNA for myocardial ischemia related gene screening

As shown in (Figure 3A–3F), the merged raw data from the three GEO datasets exhibited clear separation by dataset source; after batch correction using the ComBat algorithm, these batch effects were effectively eliminated. Subsequent differential expression analysis identified a total of 307 DEGs between myocardial ischemia and control samples (Figure 3A, 3B). Meanwhile, a co-expression network was constructed using WGCNA, a soft-thresholding power of 6 was selected, yielding 40 distinct modules (Figure 3C, Supplementary Figure S1 F–H). Module-trait relationship analysis showed that the "Green" module exhibited the highest positive correlation with the myocardial ischemia phenotype (cor = 0.38, $P = 1^{e\text{-}06}$) (Figure 3D). Furthermore, the module membership of genes in this module was significantly correlated with their gene significance for the myocardial ischemia phenotype (Figure 3E, 3F). Finally, a total of 1217 disease genes were obtained for downstream analysis by merging the 307 DEGs and the key WGCNA module genes.

Prediction of core therapeutic targets of QXD against myocardial ischemia

A total of 23 active compounds in QXD were identified through UPLC-Q-Exactive-MS analysis and target prediction across multiple databases yielded 4,535 potential protein targets for these compounds. After intersecting these targets with the 1,217 myocardial ischemia-associated genes, 329 overlapping genes were identified as the core targets through which QXD may exert therapeutic effects against myocardial ischemia (Figure 3G).

Functional enrichment analysis of core targets

As shown in the bubble and bar charts, KEGG pathway enrichment analysis indicated that the core targets were significantly enriched in the TNF signaling pathway, apoptosis, the NF-κB signaling pathway,

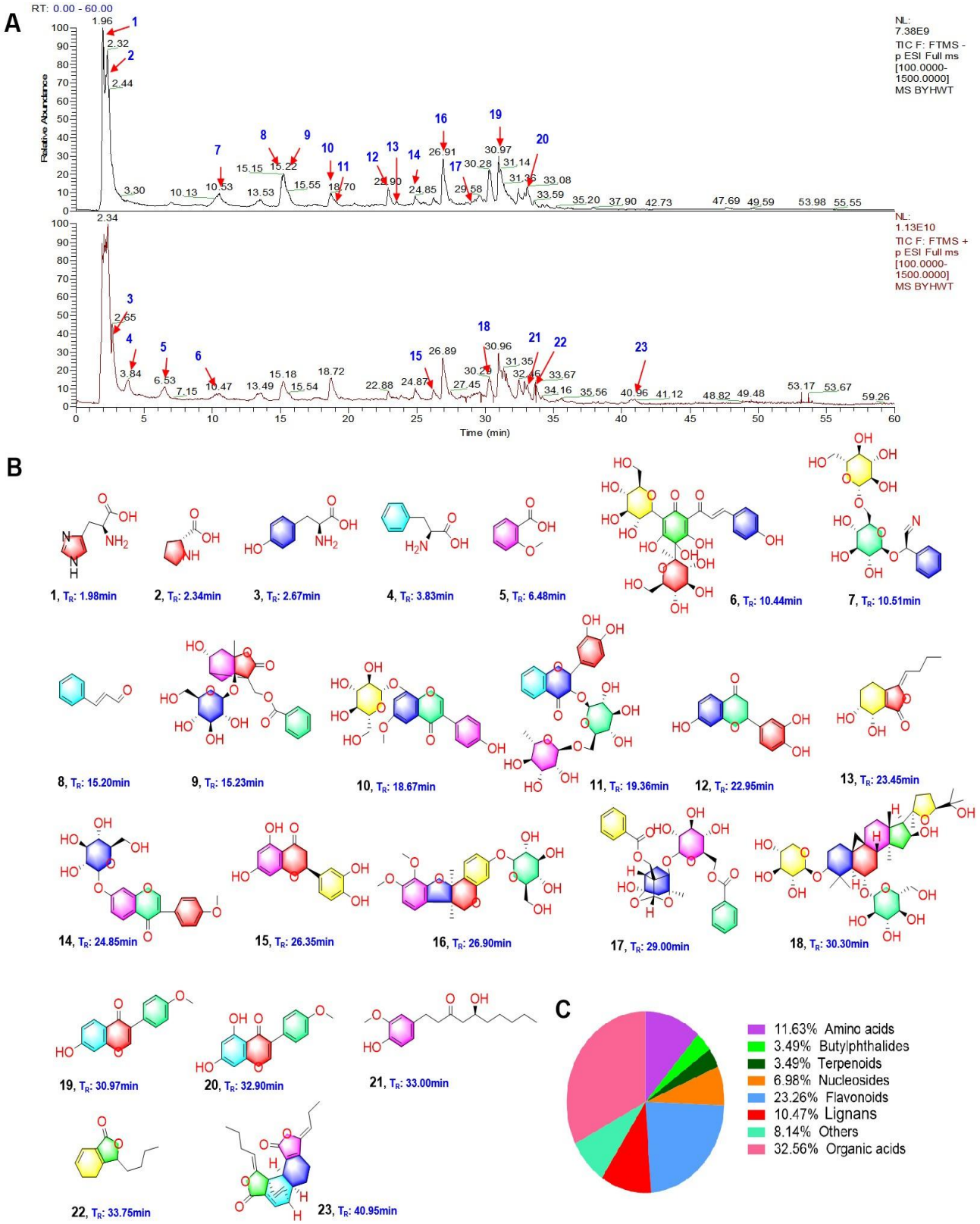

Figure 2 Constituents in QXD identified by UPLC-Q-Exactive Orbitrap-MS.

(A) Total-ion chromatogram (TIC) of UPLC-MS analysis of QXD, including Negative ion mode (upper) and Positive ion mode (lower). (B) Structures of the identified compounds. (C) Classification and proportion of compounds. UPLC, ultra-performance liquid chromatography; Q-Exactive Orbitrap-MS, quadrupole-Exactive Orbitrap mass spectrometry; TIC, total-ion chromatogram; RT, retention time; ESI, electrospray ionization; FTMS, Fourier transform mass spectrometry; QXD, Qi-Xiong-Qu-Yu decoction.

Table 1 Compounds identification from the QXD by UPLC-Q-Exactive Orbitrap-MS

No.	Compound	MF	Ionmode	RT(min)	Exp.(m/Z)	Cal.(m/z)	error	Fragmen tions
1	L-Histidine	$C_6H_9N_3O_2$	$[M+H]^+$	1.98	156.0766	156.0773	–4.48	93.0450, 110.07145, 156.07661, 156.07661
2	D-(+)-Proline	$C_5H_9NO_2$	$[M+H]^+$	2.34	116.0707	116.0712	–4.31	70.06569, 68.04995, 116.07074
3	L-Tyrosine	$C_9H_{11}NO_3$	$[M+NH_4]^+$	2.67	199.1071	199.1077	–3.01	91.05464, 119.04927, 136.07559, 165.05453
4	L-Phenylalanine	$C_9H_{11}NO_2$	$[M-H]^-$	3.83	164.0718	164.0722	–2.44	72.00795, 118.06536, 147.04419, 164.07076
5	2-Anisic acid	$C_8H_8O_3$	$[M-H]^-$	6.48	151.0394	151.0400	–3.97	59.01276, 93.03349, 123.04411, 136.01556, 151.03922
6	Safflomin A	$C_{27}H_{32}O_{15}$	$[M-H]^-$	10.44	595.1667	595.1668	–0.24	119.04913, 205.01308, 325.07147, 491.11893
7	D(-)-Amygdalin	$C_{20}H_{27}NO_{11}$	$[M+FA-H]^-$	10.51	502.1558	502.1566	–1.59	89.02328, 179.05507, 221.06627, 323.09781
8	trans-Cinnamaldehyde	C_9H_8O	$[M+H]^+$	15.20	133.0647	133.0653	–4.51	105.07014, 115.05443, 133.06477
9	albiflorin	$C_{23}H_{28}O_{11}$	$[M+FA-H]^-$	15.23	525.1623	525.1614	1.71	121.0284
10	Glycitin	$C_{22}H_{22}O_{10}$	$[M+H]^+$	18.67	447.1280	447.1292	–2.68	213.05408, 225.05443, 270.05200, 285.07544
11	Rutin	$C_{27}H_{30}O_{15}$	$[M-H+HAc]^-$	19.36	651.1555	651.1567	– 1.80	175.0387, 255.02948, 271.02441, 300.02713, 609.14526,
12	3',4,7-Trihydroxyflavanone	$C_{15}H_{12}O_5$	$[M+H]^+$	22.95	273.0752	273.0762	–3.69	135.04410, 153.01843, 271.06137
13	Senkyunolide H	$C_{12}H_{16}O_4$	$[M+H]^+$	23.45	225.1125	225.1127	–0.89	91.05466, 105.0336, 119.08566, 189.09087, 207.10139
14	Ononin	$C_{22}H_{22}O_9$	$[M-H]^-$	24.85	429.1197	429.1190	1.60	254.05717, 269.08057
15	Eriodictyol	$C_{15}H_{12}O_6$	$[M-H]^-$	26.35	287.0558	287.0562	–1.35	107.01274, 135.04413, 151.00270,
16	Methylnissolin-3-O-glucoside	$C_{23}H_{26}O_{10}$	$[M+NH_4]^+$	26.9	480.1845	480.1864	-3.96	152.04669, 167.07018, 301.10663
17	Benzoylpaeoniflorin	$C_{30}H_{32}O_{12}$	$[M+H]^+$	29.00	585.1972	585.1972	0.01	105.03377, 151.07529, 179.07013, 249.07549
18	Astragaloside IV	$C_{41}H_{68}O_{14}$	$[M+Na]^+$	30.30	807.4581	807.4592	–1.33	71.01270, 783.45264, 621.39691
19	Formononetin	$C_{16}H_{12}O_4$	$[M+H]^+$	30.97	269.0806	269.0813	–2.60	107.04939, 118.04142, 197.05965, 213.09085, 269.08047
20	5,7-dihydroxy-3-(4-methoxy phenyl)-4H-chromen-4-one	$C_{16}H_{12}O_5$	$[M+H]^+$	32.90	285.0754	285.0762	–2.88	149.02319, 170.02087, 229.08591, 285.07550
21	6-Gingerol	$C_{17}H_{26}O_4$	$[M-H]^-$	33.00	293.1757	293.1758	–0.46	221.15417, 236.10477, 96.95914
22	Senkyunolide A	$C_{12}H_{16}O_2$	$[M+H]^+$	33.75	193.1223	193.1229	–3.04	93.07033, 137.05968, 147.11674, 175.11188
23	Levistilide A	$C_{24}H_{28}O_4$	$[M+H]^+$	40.95	381.2055	381.2065	–2.63	135.04393, 191.10640, 381.20596

MF, Molecular formula; RT, retention time.

and the MAPK signaling pathway, suggesting their potential involvement in inflammation, immunity, and cell death regulation (Figure 3H). Meanwhile, GO enrichment analysis further demonstrated that the core targets were mainly involved in biological processes of apoptosis regulation, the MAPK cascade, oxidative stress, and inflammatory response (Figure 3I). The enriched molecular functions were mainly associated with the binding activities of organic acids, transcription factors, ubiquitin ligases, and cytokines, and the enriched cellular components included tertiary granules, secretory granule lumen, and membrane rafts (Supplementary Figure S2A, S2B).

QXD attenuates ISO-induced cardiomyocyte apoptosis *in vivo* and *in vitro*

To investigate the anti-apoptotic effects of QXD, TUNEL staining was performed to assess cardiomyocyte apoptosis in myocardial tissues. As shown in Figure 4A, TUNEL-positive cells were rarely observed in the normal group. Conversely, ISO administration resulted in extensive TUNEL staining, indicative of pronounced cardiomyocyte apoptosis.

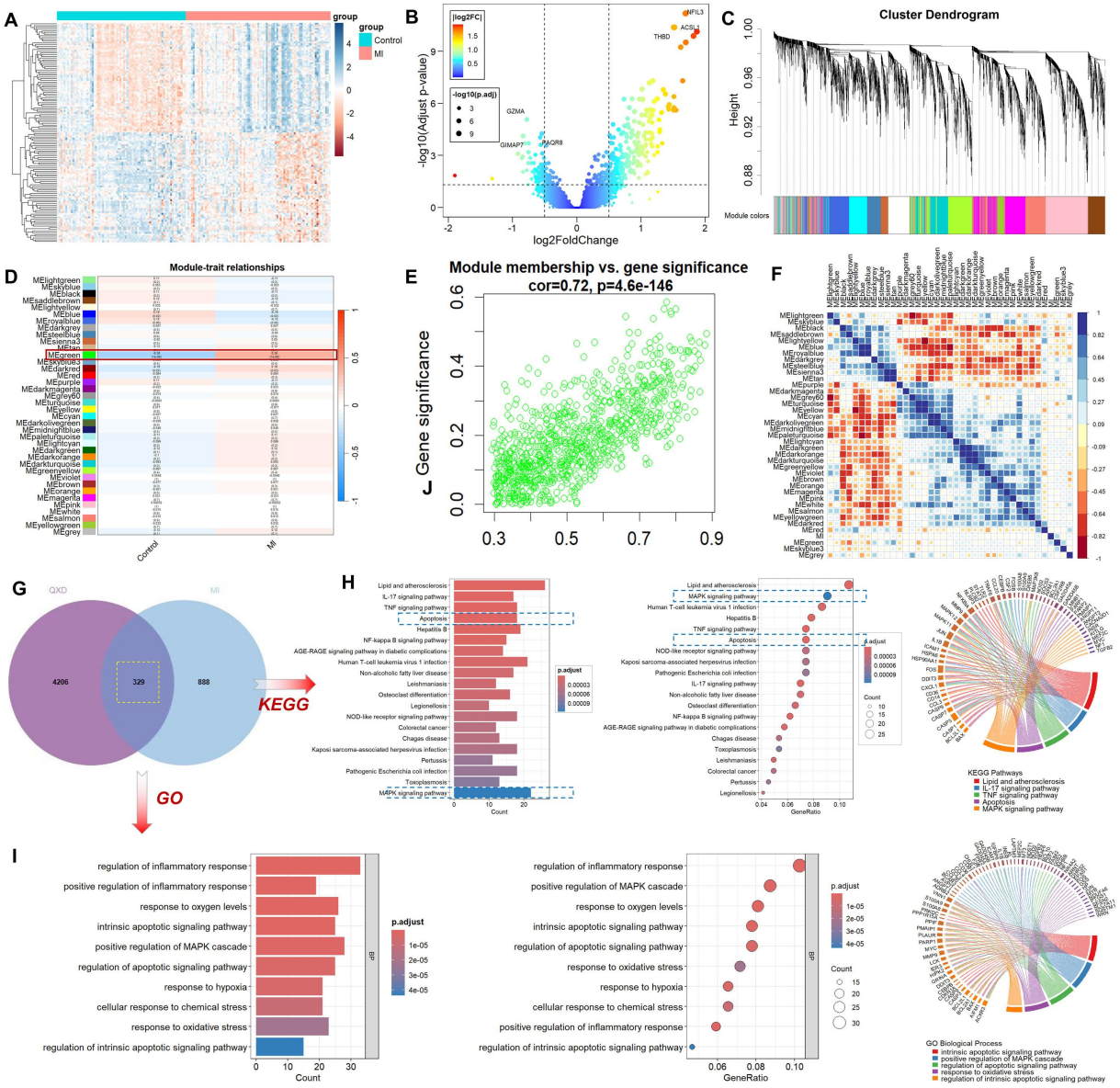

Figure 3 Core target screening and functional enrichment analysis for QXD treatment of myocardial ischemia.
(A) Heatmap showing differential expression of genes in myocardial ischemia vs. Control. (B) Volcano plot identifying significantly differentially expressed genes ($|\log_2 FC| \geq 0.5$ and $P/FDR < 0.05$). (C) Hierarchical dendrogram from weighted gene co-expression network analysis (WGCNA) indicating gene co-expression modules. (D) Heatmap depicting correlations between gene modules and the myocardial ischemia phenotype. (E) Scatter plot showing the relationship between gene significance and module membership in key modules (e.g. Green). (F) Heatmap displaying inter-module gene expression correlations. (G) Venn diagram comparing predicted QXD targets with myocardial ischemia-related genes to identify core therapeutic targets. (H) Top 20 enriched KEGG pathways. (I) GO-BP enrichment analysis of core targets. WGCNA, weighted gene co-expression network analysis; KEGG, Kyoto Encyclopedia of Genes and Genomes; GO-BP, Gene Ontology-Biological Process; QXD, Qi-Xiong-Qu-Yu decoction.

QXD treatment visibly reduced TUNEL-positive cells in a dose-dependent manner compared with the model group. Similarly, the positive control drug markedly attenuated ISO-induced apoptosis, exhibiting TUNEL fluorescence intensity comparable to that of the QXD-treated groups.

Consistent with these histological findings, Western blot analysis showed that ISO treatment significantly decreased Bcl-2 and increased BAX protein levels, thereby reducing the Bcl-2/BAX ratio ($P < 0.05$ vs control) (Figure 4B, 4C). Moreover, ISO exposure significantly upregulated cleaved caspase-3 and cleaved PARP1 expression ($P < 0.05$ vs control), whereas total caspase-3 levels remained unchanged across all groups (Figure 4D–4F). Notably, QXD treatment (800 mg/kg) significantly reversed these apoptotic alterations, as reflected by restoration of the Bcl-2/BAX ratio and suppression of cleaved caspase-3 and PARP1 expression ($P < 0.05$ vs model).

Myocardial apoptosis is commonly attributed to the excessive oxidative stress induced by ischemic state. In this study, MDA, SOD and GSH-Px levels in the myocardial tissues of myocardial ischemia rats were measured. ISO treatment induced excessive MDA accumulation and reduced the activities of the antioxidative enzymes SOD and GSH-Px in myocardial tissues ($P < 0.05$, vs. normal rats), whereas QXD significantly ameliorated oxidative stress, as evidenced by lower MDA levels and higher SOD and GSH-Px activities ($P < 0.05$, vs. model rats) (Figure 4G–4I). In addition, given that the oxidative stress and cell apoptosis are closely associated with mitochondrial structure and function, the myocardial mitochondrial ultrastructure

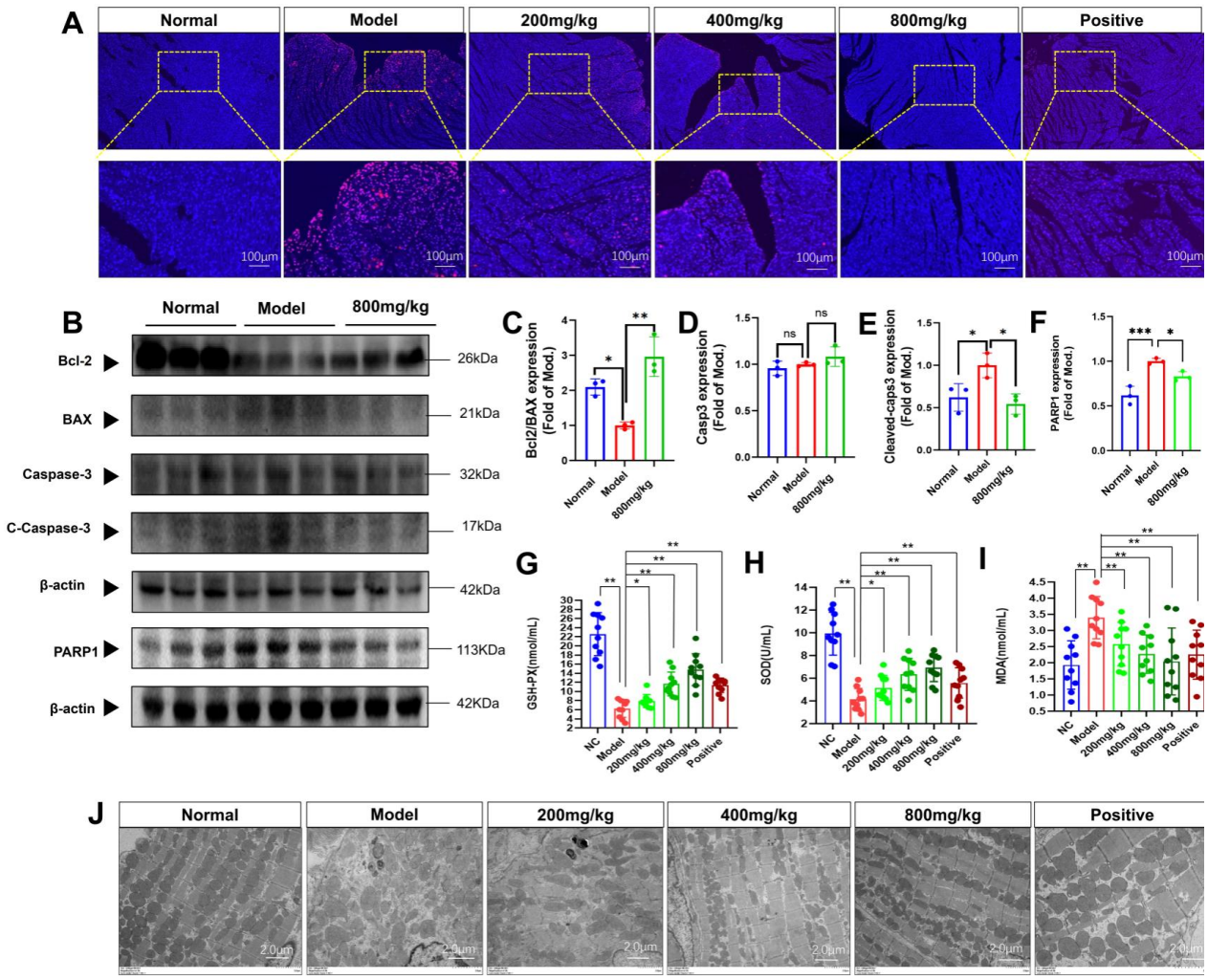

Figure 4 TUNEL and oxidative stress assays in cardiac tissues of myocardial ischemia rats.
(A) TUNEL assays. (B–F) Western blotting assays of the apoptosis related proteins. (G–I) Oxidative stress related biomarkers assays (n = 10). (J) TEM observation (n = 3). Data were expressed as Mean ± SD, $^{*}P < 0.05$, $^{**}P < 0.01$, $^{***}P < 0.001$ vs. model group; ns, not significant.

was observed by TEM in our present study (Figure 4J). Compared with the normal group, rats in the myocardial ischemia model group showed markerd degeneration and necrosis of cardiomyocytes , disorganized muscle bundles, disrupted sarcomeric structures, blurred Z-lines , abnormal aggregation of myofilaments. Mitochondrial swelling, accumulation of autophagic vacuoles/autophagosomes, interstitial fibrous tissue proliferation, and obvious macrophage infiltration were also observed. Notably, all of these pathological changes were ameliorated by QXD treatment, as evidenced by regular sarcomeric organization, preserved myo-architecture, distinct Z-lines, largely normal mitochondria with only minor swelling, and minimal interstitial fiber proliferation.

Furthermore, the anti-apoptotic effects of QXD were examined in ISO-stimulated H9C2 cells, a cell model commonly used to mimic myocardial ischemia. Flow cytometry results showed that QXD significantly decreased ISO-induced apoptosis in H9C2 cells ($P < 0.01$) (Figure 5A, 5B). In addition, QXD reduced the leakage of CK-MB, cTnT, and LDH from H9C2 cells compared with ISO-stimulated cells ($P < 0.05$) (Figure 5C–5E). Consistent with the animal experimental results, QXD treatment also reversed the ISO-induced increase in MDA and decrease in SOD in H9C2 cells ($P < 0.01$) (Figure 5F, 5G). To further explore the mechanisms underlying the anti-myocardial ischemia effects of QXD, intracellular ROS levels in ISO-stimulated H9C2 cells were measured, and QXD was found to reduce ISO-induced ROS accumulation compared with the model cells (Figure 5H).

QXD activated Nrf2 signaling and inhibited MAPK phosphorylation in ISO-stimulated H9C2 cells

Based on the network pharmacology results, MAPK signaling-related proteins were examined in ISO-stimulated H9C2 cells. The results showed that ISO treatment activated MAPK signaling by increasing the phosphorylation of the MAPK proteins p38, JNK, and ERK compared with normal H9C2 cells ($P < 0.01$), whereas QXD treatment markedly reduced the phosphorylation of p38, JNK, and ERK ($P < 0.01$) (Figure 6A–6K). Furthermore, the nuclear accumulation of Nrf2, a well-known transcription factor regulating the production of antioxidative enzymes, was assessed in ISO-stimulated H9C2 cells. The results indicated that QXD significantly promoted the nuclear accumulation of Nrf2 ($P < 0.01$) (Figure 6L–6P) and up-regulated the expression of the antioxidative enzyme HO-1 compared with the model cells ($P < 0.01$) (Figure 6M, 6Q).

Plasma metabolomic analysis of QXD-treated myocardial ischemia rats

Plasma metabolomic analysis is beneficial for revealing the overall molecular mechanism profile. In the present study, partial least squares-discriminant analysis (PLS-DA) was performed in both positive and negative ion modes, and the score plots with 95% confidence ellipses showed separation between the model and

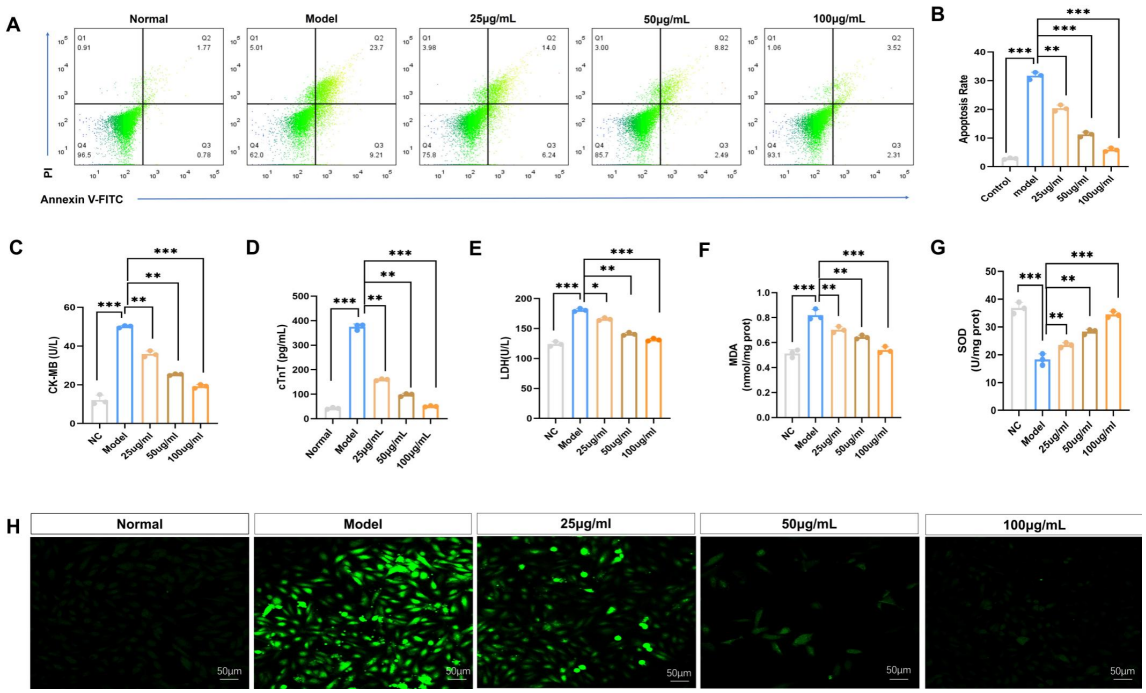

Figure 5 Effects of QXD on ISO-stimulated H9C2 cells.

(A, B) Apoptotic determination in ISO-stimulated H9C2 cells via flow cytometry by staining with Annexin V-FITC/PI. (C–E) Myocardial injury biomarkers levels of CK-MB, cTnT and LDH in cell supernatant. (F, G) MDA and SOD levels in ISO-stimulated H9C2 cells. (H) ROS levels in ISO-stimulated H9C2 cells. Data were expressed as Mean ± SD (n = 3), $^{*}P < 0.05$, $^{**}P < 0.01$, $^{***}P < 0.001$ vs. Model group. NC, normal control; CK-MB, creatine kinase-MB; cTnT, cardiac troponin T; LDH, lactate dehydrogenase; MDA, malondialdehyde; SOD, superoxide dismutase; ROS, reactive oxygen species; ISO, isoproterenol; QXD, Qi-Xiong-Qu-Yu decoction; ns, not significant.

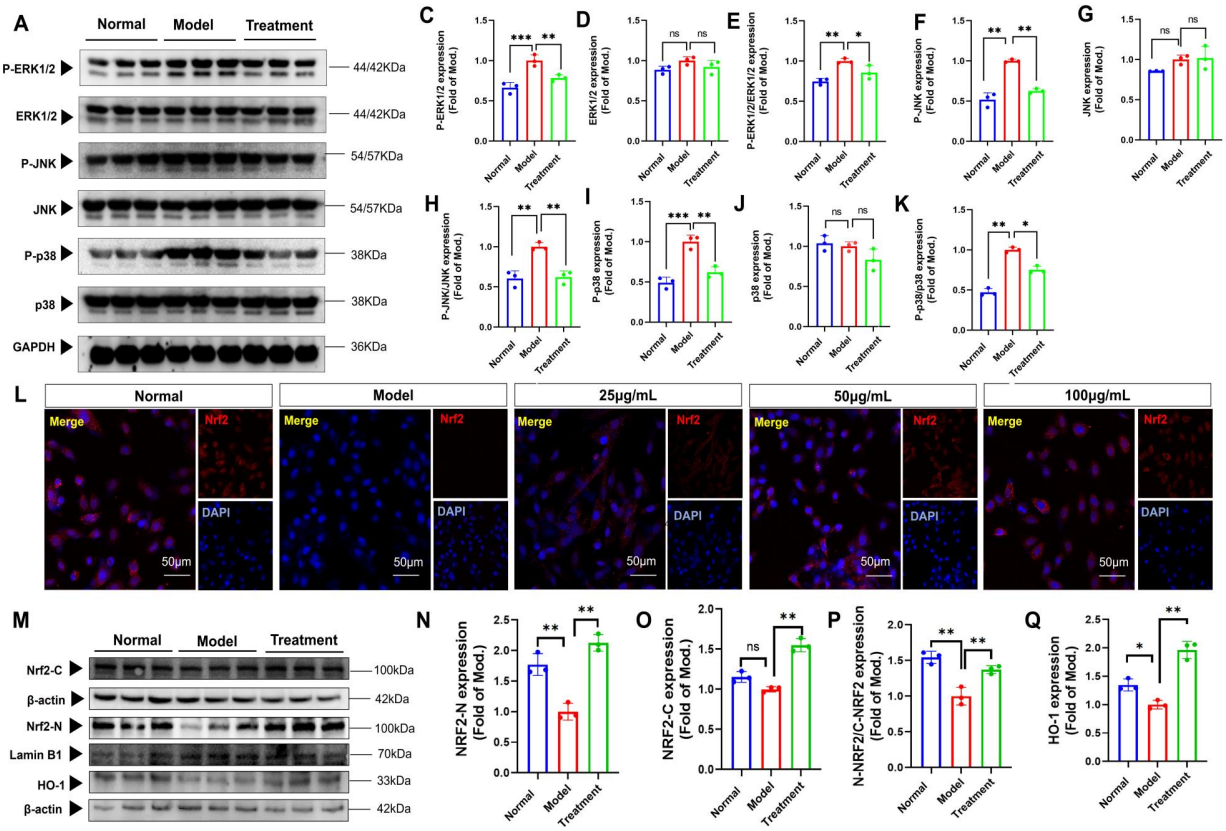

Figure 6 Effects of QXD on Nrf2/MAPK signaling in ISO-stimulated H9C2 cells.

(A–K) Western blotting assays of MAPK signaling. (L) Determination of the nuclear accumulation of Nrf2 by laser confocal observation. (M–Q) Western blotting assays of the Nrf2. Data were expressed as Mean ± SD (n = 3), $^{*}P < 0.05$, $^{**}P < 0.01$, $^{***}P < 0.001$ vs. Model group; ns, not significant. QXD, Qi-Xiong-Qu-Yu decoction.

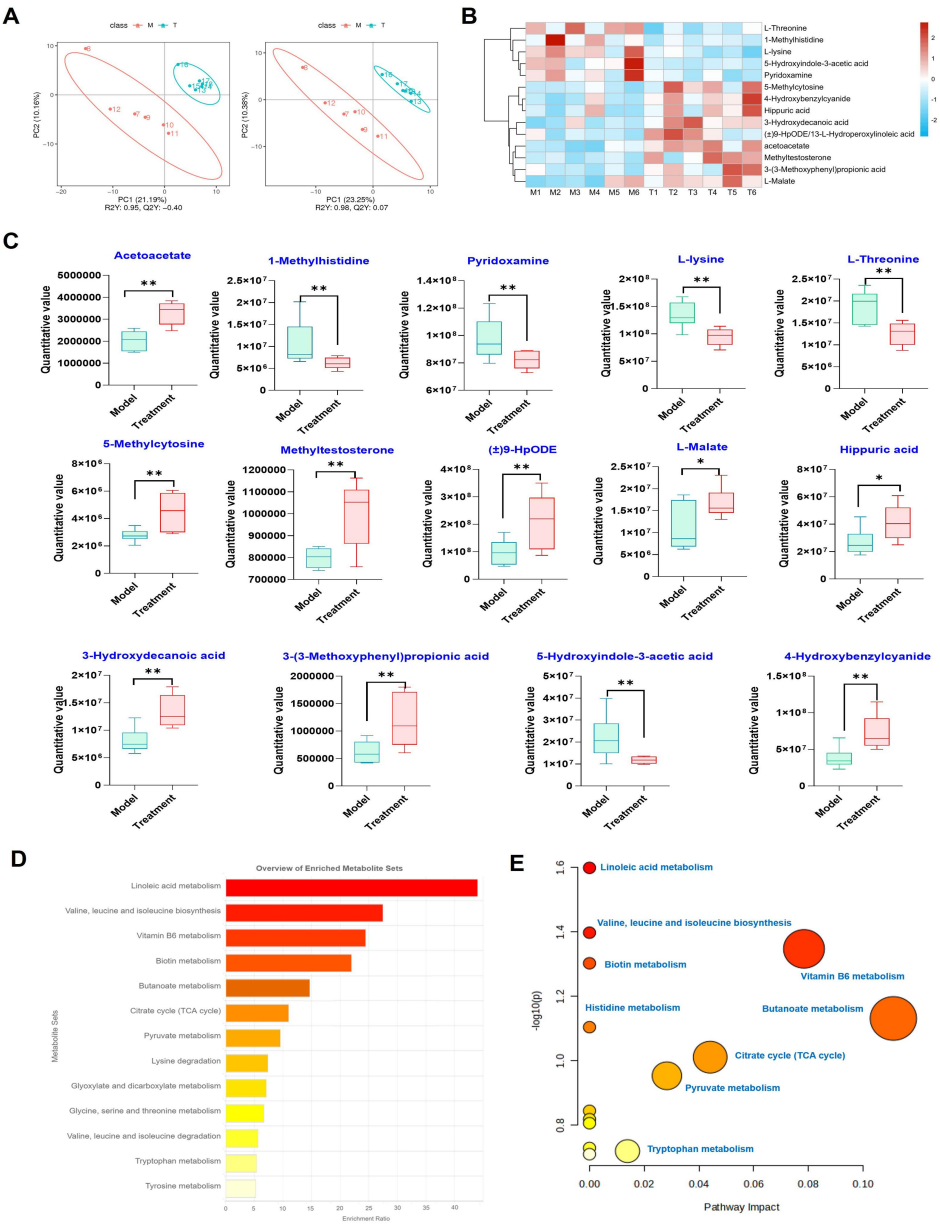

Figure 7 Metabolomic analysis for treating myocardial ischemia in rats.
(A) PLS-DA score plots of metabolites in positive (left) and negative (right) ion modes between the model and QXD-treated groups with 95% confidence ellipses. (B) Clustering heat map analysis of metabolites. (C) Abundance of differential metabolites in enriched pathways. (D) Enrichment of metabolites; (E) Enrichment analysis of metabolic pathways. Data were expressed as Mean ± SD (n = 6), $^{*}P < 0.05$, $^{**}P < 0.01$ vs. Model group. PLS-DA, partial least squares-discriminant analysis. M, model group; T, QXD-treated group. QXD, Qi-Xiong-Qu-Yu decoction.

QXD-treated groups (Figure 7A). Fourteen differential endogenous metabolites were screened from the plasma of QXD-treated myocardial ischemia rats according to multivariate statistical criteria —variable importance in projection (VIP) ≥ 1.0, fold change (FC) ≥ 2.0 or ≤ 0.5, and $P < 0.05$ — comprising 9 up-regulated and 5 down-regulated metabolites compared with the model rats (Figure 7B, 7C). Among them, 9-HpODE and 5-hydroxyindole-3-acetic acid showed the most significant changes. Metabolite set enrichment analysis was then performed using MetaboAnalyst 5.0 to delineate the QXD-regulated metabolic pathways implicated in myocardial ischemia pathogenesis. As illustrated in Figure 7D, 7E, linoleic acid metabolism, valine/leucine/isoleucine biosynthesis, vitamin B6 metabolism, and butyrate metabolism were identified as the key biochemical networks. To strengthen the integration of network pharmacology and metabolomics, joint pathway analysis of the 329 core targets and the 14 differential metabolites was performed (Supplementary Figure S4). The two omics datasets converged on several pathways closely related to myocardial ischemia pathogenesis, including the MAPK signaling pathway, linoleic acid metabolism, arachidonic acid metabolism, glutathione metabolism, and ferroptosis. Notably, linoleic acid metabolism directly connects the differential metabolite 9-HpODE with thetarget PLA2G6, while the MAPK signaling pathway was the most significantly enriched pathway among the core targets, together providing an integrated mechanistic basis linking the QXD-regulated metabolites to the Nrf2/ROS/MAPK signaling axis.

Discussion

Myocardial ischemia remains one of the most common chronic heart diseases in clinical practice, imposing a substantial global burden [2, 24]. Meanwhile, ever-changing dietary habits and lifestyles have been

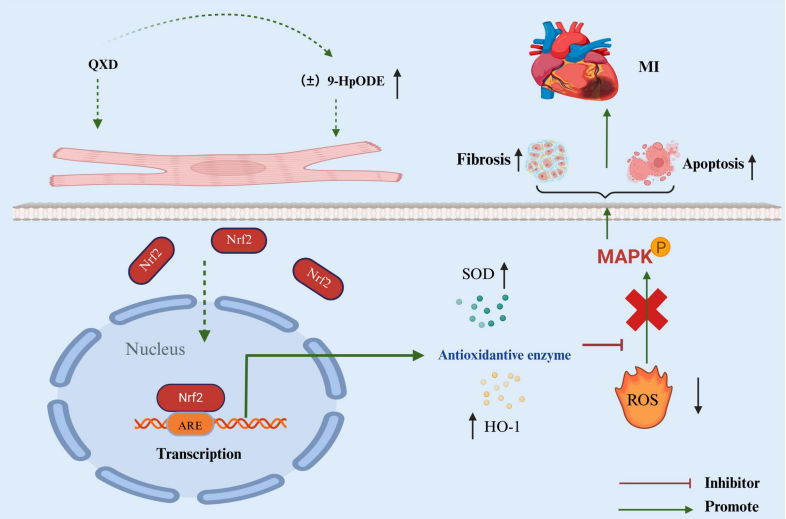

Figure 8 Mechanism of action of QXD in the treatment of myocardial ischemia.
QXD, Qi-Xiong-Qu-Yu decoction.

increasingly recognized as important modifiable risk factors contributing to the rising incidence of cardiovascular diseases [2]. Nowadays, TCMs and their formulas (TCMFs) have attracted growing attention owing to their diverse bioactive constituents and demonstrated therapeutic potential [25, 26]. QXD is a clinically experienced, self-designed formula used to treat various chronic cardiovascular diseases. In the present study, we evaluated the anti-myocardial ischemia effects of QXD using an ISO-induced myocardial ischemia rat model [27], and further explored the underlying molecular mechanisms by integrating multi-omics analyses with *in vitro* cell experiments.

It is well established that excessive ROS are directly correlated with the development of myocardial ischemia, and excessive ROS can lead to apoptosis, fibrosis and inflammation in myocardial tissues [28–30]. In the present study, we found that QXD can not only ameliorated the elevated serum levels of the myocardial injury biomarkers cTnT, CK-MB and LDH in myocardial ischemia rats, but also the alleviated the pathological changes and fibrosis in myocardial tissues. Furthermore, our results indicated that QXD attenuated apoptosis in the myocardial tissues of myocardial ischemia rats. Because the high-dose ISO regimen induces both coagulative necrosis and apoptosis in myocardial tissues, apoptotic cell death was specifically verified through complementary approaches: TUNEL-positive cells were quantified in the peri-infarct border zone rather than the necrotic core, apoptosis-specific molecular markers (the Bcl-2/Bax ratio, cleaved caspase-3, and PARP1) were examined, and Annexin V/PI flow cytometry was applied in H9C2 cells to distinguish early apoptotic cells (Annexin V^+/PI^-) from necrotic or late apoptotic cells (Annexin V^+/PI^+). Mechanistic investigation showed that QXD treatment was associated with reduced ROS accumulation in ISO-induced cardiomyocytes. UPLC-MS/MS analysis showed that QXD contains abundant natural compounds rich in hydroxyl groups (including flavonoids and terpenoids), such as safflomin A, albiflorin, glycitin, rutin, ononin, benzoylpaeoniflorin, astragaloside IV, and formononetin, which possess potent radical-scavenging activities and can eliminate ROS in myocardial tissues. Nrf2 signaling plays a crucial role in maintaining redox homeostasis by promoting the production of multiple antioxidant enzymes, such as HO-1, SOD, and GSH-Px [31]. In this study, QXD treatment was associated with increased Nrf2 nuclear accumulation and alleviated oxidative stress, as evidenced by reduced ROS levels and improved redox balance. These findings imply a potential involvement of Nrf2-related antioxidant responses in the protective effects of QXD against ISO-induced injury; however, due to the absence of Nrf2 knockout or specific pathway inhibitors, the causal relationship between Nrf2 activation and the observed antioxidant effects remains to be established in future studies. Network pharmacological analysis also predicted that QXD could regulate MAPK signaling in myocardial cell. In addition, MAPK signaling acts upstream of apoptosis, inflammation and fibrosis in cardiomyocytes [32, 33]. Notably, ROS are upstream signaling molecule that triggers the activation and phosphorylation of the MAPK pathway [34, 35] and its downstream apoptotic events [36]. Consistently, our results demonstrated that QXD inhibited the phosphorylation of MAPK signaling molecules , including p38, JNK and ERK1/2.

In addition, plasma metabolomic analysis suggested that QXD treatment moderately up-regulated the endogenous metabolite of 9-HpODE (9(S)-hydroperoxy-10(E),12(Z)-octadecadienoic acid) in plasma and regulated the linoleic acid metabolic pathway. Previous studies have suggested that moderately elevated 9-HpODE, an intermediate of the linoleic acid metabolic pathway, may activate Nrf2 signaling and promote the nuclear accumulation of Nrf2, thereby regulating redox homeostasis [37]. Thus, our results also suggest that QXD may regulate the endogenous metabolites such as 9-HpODE to potentially activate Nrf2 signaling, which may further contribute to the suppression of inflammation, fibrosis and apoptosis in myocardial tissues.

Conclusion

In summary, the present study demonstrates that QXD can mitigate isoproterenol-induced experimental myocardial ischemia in rats, and the underlying molecular mechanisms are closely associated with the suppression of cardiomyocyte apoptosis through the regulation of Nrf2/ROS/MAPK signaling (Figure 8). In addition, the findings of this study provide a valuable basis for future new drug development and the promotion of clinical applications of QXD.

References

1. Liu CL, Jin QF, Han CX, Jiao M. Global, regional, and national burden of ischaemic heart disease from 1990 to 2021: a comprehensive analysis based on the Global Burden of Disease study 2021. *J Glob Health*. 2025;15:04291. Available at: https://doi.org/10.7189/jogh.15.04291
2. Roth GA, Mensah GA, Johnson CO, et al. Global Burden of Cardiovascular Diseases and Risk Factors, 1990–2019: Update From the GBD 2019 Study. *J Am Coll Cardiol*. 2020;76(25):2982–3021. Available at: https://doi.org/10.1016/j.jacc.2020.11.010

3. Benjamin EJ, Muntner P, Alonso A, et al. Heart Disease and Stroke Statistics—2019 Update: A Report From the American Heart Association. *Circulation*. 2019;139(10):e56–e528. Available at: https://doi.org/10.1161/CIR.0000000000000659
4. Vasan RS, Benjamin EJ. The future of cardiovascular epidemiology. *Circulation*. 2016;133(25):2626–2633. Available at: https://doi.org/10.1161/CIRCULATIONAHA.116.023528
5. Bangalore S, Bhatt DL, Steg PG, et al. β-Blockers and Cardiovascular Events in Patients With and Without Myocardial Infarction: An International Cohort Study. *Circ Cardiovasc Qual Outcomes*. 2014;7(5):720–730. Available at: https://doi.org/10.1161/CIRCOUTCOMES.114.001073
6. Fordham M, Lyubarova R, Sidhu M. The Beta-Blocker Dilemma: Revisiting Their Role in Cardiovascular Disease. *Cardiovasc Drugs Ther*. 2025;39(5):941–943. Available at: https://doi.org/10.1007/s10557-025-07678-1
7. Hao PP, Jiang F, Cheng J, Ma L, Zhang Y, Zhao Y. Traditional Chinese Medicine for Cardiovascular Disease: Evidence and Potential Mechanisms. *J Am Coll Cardiol.* 2017;69(24):2952–2966. Available at: https://doi.org/10.1016/j.jacc.2017.04.041
8. Li WC, Liu X, Liu Z, et al. Therapeutic potential of traditional Chinese medicine in diabetic cardiomyopathy: a review. *Front Endocrinol (Lausanne)*. 2025;16:1532565. Available at: https://doi.org/10.3389/fendo.2025.1532565
9. Zhang L, Zheng CL, Jiang M, et al. Effect of Yiqi Huoxue Decoction on the metabolomics of acute myocardial infarction rats. *J Tradit Chin Med Sci.* 2017;4(2):195–206. Available at: https://doi.org/10.1016/j.jtcms.2017.06.001
10. Bai XY, Wei H, Liu GQ, Li L. Astragalus polyphenols attenuates doxorubicin-induced cardiotoxicity by activating the PI3K/AKT/NRF2 pathway. *PLoS One.* 2025;20(2):e0319067. Available at: https://doi.org/10.1371/journal.pone.0319067
11. Hou M, Leng YF, Shi YJ, Tan ZG, Min XZ. Astragalus membranaceus as a Drug Candidate for Inflammatory Bowel Disease: The Preclinical Evidence. *Am J Chin Med.* 2023;51(6):1501–1526. Available at: https://doi.org/10.1142/s0192415x23500684
12. Duan JL, Wang JW, Guan Y, et al. Safflor yellow A protects neonatal rat cardiomyocytes against anoxia/reoxygenation injury in vitro. *Acta Pharmacol Sin.* 2013;34(4):487–495. Available at: https://doi.org/10.1038/aps.2012.185
13. Wang G, Dai GL, Song J, et al. Lactone Component From Ligusticum chuanxiong Alleviates Myocardial Ischemia Injury Through Inhibiting Autophagy. *Front Pharmacol.* 2018;9:301. Available at: https://doi.org/10.3389/fphar.2018.00301
14. Zeng SY, Zhu YC, Su C, et al. Integrating serum metabolomics analysis and network pharmacology to reveal the potential mechanism of Shengmai Jianghuang San in the treatment of nasopharyngeal carcinoma. *Biomed Chromatogr.* 2024;38(10):e5981. Available at: https://doi.org/10.1002/bmc.5981
15. Zheng YN, Shi X, Hou JB, et al. Integrating metabolomics and network pharmacology to explore Rhizoma Coptidis extracts against sepsis-associated acute kidney injury. *J Chromatogr B Analyt Technol Biomed Life Sci.* 2021;1164:122525. Available at: https://doi.org/10.1016/j.jchromb.2021.122525
16. Ren CX, Gao MY, Li N, et al. Identification and mechanism elucidation of medicative diet for food therapy XQCSY in NAFLD prevention: an integrative in silico study. *Food Med Homol.* 2024;1(2):9420015. Available at: https://doi.org/10.26599/fmh.2024.9420015
17. Asdaq SMB, Inamdar MN, Asad M, Nanjundan PK. Interaction of propranolol with garlic in isoproterenol induced myocardial infarction in rat. *J Pharmacol Toxicol.* 2008;3(6):414–424. Available at: https://doi.org/10.3923/jpt.2008.414.424
18. Tsai CK, ChEN BH, Chen HH, et al. Low-Dose Propranolol Prevents Functional Decline in Catecholamine-Induced Acute Heart Failure in Rats. *Toxics*. 2022;10(5):238. Available at: https://doi.org/10.3390/toxics10050238
19. Wu ZZ, Chen X, Ye JH, Wang XY, Hu ZX. Pericarpium Trichosanthis Injection Protects Isoproterenol-Induced Acute Myocardial Ischemia via Suppressing Inflammatory Damage and Apoptosis Pathways. *Biomedicines*. 2025;15(5):618. Available at: https://doi.org/10.3390/biom15050618
20. Han X, Qi JY, Yang YK, et al. Protective mechanisms of 10-gingerol against myocardial ischemia may involve activation of JAK2/STAT3 pathway and regulation of Ca^{2+} homeostasis. *Biomed Pharmacother*. 2022;151:113082. Available at: https://doi.org/10.1016/j.biopha.2022.113082
21. Liang H, He YY, Wang YW, et al. Aldehyde Dehydrogenase-2 Alleviates Septic Myocardial Injury by Inhibiting Caspase-11-Mediated Noncanonical Pyroptosis. *CardiovascTher*. 2026; 2026:5289405. Available at: https://doi.org/10.1155/cdr/5289405
22. Long Y, Xiao Y, Chen C, Peng C, Zhang YX. The effect of astragaloside IV on a model of isoproterenol-induced hypertrophic injury in H9c2 cells. *Acta Pharm*. 2026;76(1):1–12. Available at: https://doi.org/10.2478/acph-2026-0006
23. Liu ZP, Tang WS, Wang GZ, et al. Ferulic acid inhibiting colon cancer cells at different Duke's stages. *Food Med Homol.* 2025;2(3):9420063. Available at: https://doi.org/10.26599/fmh.2025.9420063
24. Virani SS, Newby LK, Arnold SV, et al. 2023 AHA/ACC/ACCP/ASPC/NLA/PCNA Guideline for the Management of Patients With Chronic Coronary Disease: A Report of the American Heart Association/American College of Cardiology Joint Committee on Clinical Practice Guidelines. *Circulation*. 2023;148(9):e9–e119. Available at: https://doi.org/10.1161/CIR.0000000000001168
25. He CX, Wang PP, Zuo YY, et al. Constituents-composed Chinese medicine of Dajianzhong Decoction ameliorates Non-alcoholic fatty liver disease via AMPK/PPARα/CPT1 signaling. *Phytomedicine.* 2025;149:157515. Available at: https://doi.org/10.1016/j.phymed.2025.157515
26. Liang Q, Gou HH, Chen LP, He CX, Wu CJ, Peng W. "Food & medicine homology" medicines and their formulas: a versatile approach for the management of lipid metabolic disorders related diseases. *Food Med Homol.* 2026;3(1):9420130. Available at: https://doi.org/10.26599/fmh.2026.9420130
27. Mu XY, Yu HZ, Li HF, et al. Metabolomics analysis reveals the effects of Salvia Miltiorrhiza Bunge extract on ameliorating acute myocardial ischemia in rats induced by isoproterenol. *Heliyon*. 2024;10(9):e30488. Available at: https://doi.org/10.1016/j.heliyon.2024.e30488
28. Kibel A, Lukinac AM, Dambic V, Juric I, Selthofer-Relatic K. Oxidative stress in ischemic heart disease. *Oxid Med Cell Longev*. 2020;2020:6627144. Available at: https://doi.org/10.1155/2020/6627144
29. Liu C, Zhang XJ, Yang HY, et al. PEG-modified nano liposomes co-deliver Apigenin and RAGE-siRNA to protect myocardial ischemia injury. *Int J Pharm.* 2024;649:123673. Available at: https://doi.org/10.1016/j.ijpharm.2023.123673
30. Xiang M, Lu YD, Xin LY, et al. Role of Oxidative Stress in Reperfusion following Myocardial Ischemia and Its Treatments. *Oxid Med Cell Longev.* 2021;2021:6614009. Available at: https://doi.org/10.1155/2021/6614009
31. Hayes JD, Dayalan Naidu S, Dinkova-Kostova AT. Regulating

Nrf2 activity: ubiquitin ligases and signaling molecules in redox homeostasis. *Trends Biochem Sci.* 2025;50(3):179–205. Available at: https://doi.org/10.1016/j.tibs.2024.12.010

32. Wang XY, Liu RQ, Liu D. The role of the MAPK signaling pathway in cardiovascular disease: pathophysiological mechanisms and clinical therapy. *Int J Mol Sci*. 2025;26(6):2667. Available at: https://doi.org/10.3390/ijms26062667
33. Romero-Becerra R, Santamans AM, Folgueira C, Sabio G. p38 MAPK pathway in the heart: new insights in health and disease. *Int J Mol Sci*. 2020;21(19):7412. Available at: https://doi.org/10.3390/ijms21197412
34. Yao YW, Chen R, Ying CY, Zhang GH, Rui T, Tao AB. Interleukin-33 attenuates doxorubicin-induced cardiomyocyte apoptosis through suppression of ASK1/JNK signaling pathway. *Biochem Biophys Res Commun*. 2017;493(3):1288–1295. Available at: https://doi.org/10.1016/j.bbrc.2017.09.153
35. Meijles DN, Cull JJ, Markou T, et al. Redox regulation of c ardiac ASK1 (apoptosis signal-regulating kinase 1) controls p38-MAPK (mitogen-activated protein kinase) and orchestrat es cardiac remodeling to hypertension. *Hypertension*. 2020;7 6(4):1208–1218. Available at: https://doi.org/10.1161/HYPERTENSIONAHA.119.14556
36. Yue JC, Lopez JM. Understanding MAPK signaling pathways in apoptosis. *Int J Mol Sci*. 2020;21(7):2346. Available at: https://doi.org/10.3390/ijms21072346
37. Gu SM, Chen C, Wang JM, et al. Camellia Japonica Radix modulates gut microbiota and 9(S)-HpODE-mediated ferroptosis to alleviate oxidative stress against MASLD. *Phytomedicine.* 2025;143:156806. Available at: https://doi.org/10.1016/j.phymed.2025.156806